Probing the Self-Assembly Mechanism of Diphenylalanine-Based Peptide Nanovesicles and Nanotubes

Cong Guo,[†] Yin Luo,[†] Ruhong Zhou,[‡,*] and Guanghong Wei[†,*]

[†]State Key Laboratory of Surface Physics, Key Laboratory for Computational Physical Sciences (Ministry of Education), and Department of Physics, Fudan University, 220 Handan Road, Shanghai, 200433, China and [‡]IBM Thomas J. Watson Research Center, Yorktown Heights, New York 10598, United States, and Department of Chemistry, Columbia University, New York, New York 10027, United States

ABSTRACT Nanostructures, particularly those from peptide self-assemblies, have attracted great attention lately due to their potential applications in nanotemplating and nanotechnology. Recent experimental studies reported that diphenylalanine-based peptides can self-assemble into highly ordered nanostructures such as nanovesicles and nanotubes. However, the molecular mechanism of the self-organization of such well-defined nanoarchitectures remains elusive. In this study, we investigate the assembly pathway of 600 diphenylalanine (FF) peptides at different peptide concentrations by performing extensive coarse-grained molecular dynamics (MD) simulations. Based on forty 0.6—1.8 μs trajectories at 310 K starting from random configurations, we find that FF dipeptides not only spontaneously assemble into spherical vesicles and nanotubes, consistent with previous experiments, but also form new ordered nanoarchitectures, namely, planar bilayers and a rich variety of other shapes of vesicle-like structures including toroid, ellipsoid, discoid, and pot-shaped vesicles. The assembly pathways are concentration-dependent. At low peptide concentrations, the self-assembly involves the fusion of small vesicles and bilayers, whereas at high concentrations, it occurs through the formation of a bilayer first, followed by the bending and closure of the bilayer. Energetic analysis suggests that the formation of different nanostructures is a result of the delicate balance between peptide—peptide and peptide—water interactions. Our all-atom MD simulation shows that FF nanostructures are stabilized by a combination of T-shaped aromatic stacking, interpeptide head-to-tail hydrogen-bonding, and peptide—water hydrogen-bonding interactions. This study provides, for the first time to our knowledge, the self-assembly mechanism and the molecular organization of FF dipeptide nanostructures.

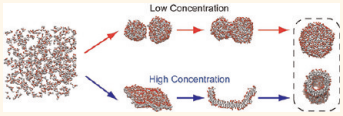

KEYWORDS: nanostructure · phenylalanine dipeptide · self-assembly pathway · coarse-grained model · molecular dynamics simulations · T-shaped aromatic stacking

Peptide self-assembly has attracted considerable attention due to its important role not only in biological processes such as amyloid fibril formation associated with numerous neurodegenerative diseases[1] but also in the design of novel nanobiomaterials.[1−4] It has been reported that cyclic peptides, amphiphilic peptides, and amyloid-inspired peptides can form ordered nanostructures with different morphologies including nanotubes, nanovesicles, nanofibrils, and nanosheets.[5−9] Among these various peptide building blocks, diphenylalanine peptide has been extensively studied experimentally due to its structural simplicity, functional versatility, and broad applications[10,11] in biology (such as drug delivery, bioimaging, biosensors) and in nanotechnology (as templates for the fabrication of metal nanowires and functional polymer nanotubes).[12−16] L-Phe-L-Phe (FF) peptide was initially reported to form pore-size hydrophilic nanochannels when crystallized.[17] It was further shown to form nanotubes in solution upon dilution from organic solvents into aqueous solution.[6,18−20] Under a similar synthesis procedure, its D-amino acid analogue, D-Phe-D-Phe, was reported to form nanotubes with the same structural features as the corresponding L-amino acid FF peptide. When the preparation method of D-Phe-D-Phe nanotube was simplified by omitting the organic solvent, it was observed that the nanotubes turned into vesicles upon diluting the peptide nanotube solution.[21] Since the emergence of FF dipeptide as a self-assembling building block, many studies have also been performed on other FF-based dipeptides including cationic FF, Fmoc-FF, and the diphenylglycine peptide. These FF-based building blocks can assemble into nanotubes and other nanoarchitectures such as vesicles, nanofibrils, nanowires, and ribbons.[2,11,21−23]

The polymorphism of ordered nanostructures is affected by many factors such as the type of solvents, peptide concentration, the pH value, and temperature.[11] Among them, peptide concentration has been reported to play a critical role in determining the final nanostructure morphology. For example, the spontaneous transformation of nanotubes

* Address correspondence to ghwei@fudan.edu.cn; ruhongz@us.ibm.com.

Received for review January 3, 2012 and accepted April 2, 2012.

Published online April 02, 2012
10.1021/nn300015g

into vesicles takes place by diluting the D-Phe-D-Phe peptide solution,[21] and the cationic FF peptide was reported to form nanotubes at high peptide concentrations[24−26] but to adopt vesicles at low peptide concentrations.[25,26]

Although significant advances have been made in the study of FF-based peptide nanoarchitectures, the assembly pathway and the detailed structural information of the ordered nanostructures remain to be determined. Such knowledge is important for elucidating the molecular mechanism of FF-based dipeptide nanostructure formation and provides insight into the precise control of the peptide assembly for targeted biological applications. Because of its short amino acid length, its important role in the fibril formation of the Alzheimer's β-amyloid (Aβ) peptide, and its ability to assemble into well-defined nanostructures,[6,27] FF as well as the corresponding D-amino acid dipeptides has been studied computationally in an attempt to understand the fibrillization mechanism of Aβ peptide and to obtain insights into the interactions and structural properties of the FF nanostructures using both all-atom[28,29] and coarse-grained (CG) peptide models.[30,31] In those studies, only disordered aggregates were obtained, probably due to the small size of the studied systems (up to 96 FF chains) and/or the short simulation time ($\leq$40 ns for all-atom molecular dynamics (MD) simulations and $\leq$5 ns for CG MD simulations). Although nanovesicles and nanotubes were sampled at different peptide concentrations in an earlier study on D-Phe-D-Phe peptides using Monte Carlo simulations with a highly simplified one-parameter lattice model (32 $\times$ 32 $\times$ 32),[21] a detailed self-assembly process into ordered nanostructures was still missing.[4,11,27] Overall, in spite of the enormous potential applications of FF-based nanomaterials and the emergence of a few computational studies on the FF-based dipeptides, there is still "a notable lack of theoretical insight into peptide nanostructure formation".[11,27]

In this work, we investigate the assembly mechanism of 600 FF dipeptides at four different peptide concentrations and probe the structural characteristics of the spontaneously assembled aggregates by performing extensive MD simulations. As simulating the formation of FF nanostructures with all-atom models is extremely challenging computationally because of the large system sizes and the long time scales needed to understand the assembly process starting from a random conformation, we used the MARTINI CG model[32,33] to achieve a quantitative approximation of the atomic behavior while easing the computational requirements for simulation. The current study with detailed analysis of 40 long-time independent trajectories highlights several findings that in particular address the structures of assemblies and the course of primary events during the peptide assembly process. First, consistent with previous experimental observations,[6,11,20,22] ordered nanostructures such as spherical vesicles and nanotubes are observed in our MD trajectories, and a transformation from vesicle-like to tubular structures is seen at high peptide concentration. Second, new well-defined nanoarchitectures are identified, namely, planar two-dimensional bilayers and vesicle-like structures with a rich variety of shapes including toroid, ellipsoid, discoid, and pot-shaped vesicles. Third, our simulations show that the assembly pathways of FF dipeptides into vesicles/tubes are concentration-dependent. At low concentrations, the spontaneous formation of FF-based peptide nanostructures involves the fusion of vesicles or the fusion of vesicles with a bilayer, whereas at high concentrations, the self-assembly occurs through the formation of a bilayer first, followed by the bending and closure of the bilayer. Fourth, we found that an aromatic stacking interaction is the dominant driving force for the self-organization, and the exact structure formation depends on the balance between peptide−peptide and peptide−water interactions. Finally, all-atom MD simulations on a fine-grained structure of a spherical vesicle from the CG MD trajectory demonstrate that two adjacent aromatic rings in the ordered nanostructures have a strong preference to adopt a T-shaped orientation.

TABLE 1. Summary of the Simulation Results

peptide concentration (mg/mL)	total no. of MD runs	no. of MD runs generating a structure		
		vesicle-like	nanotube	bilayer
50	10	10	0	0
85	10	7	2	1
120	10	3	3	4
155	10	0	1	9

RESULTS AND DISCUSSION

A rich variety of ordered nanostructures are observed in our extensive CG MD simulations. We classify these nanostructures into three families: vesicle-like structure if it is closed in three dimensions (3D), nanotube if it is closed in two dimensions (2D), and bilayer if it is not closed. Table 1 summarizes these nanostructures from our MD simulations at various concentrations. It can be seen that the morphology of the FF nanostructure is concentration-dependent. At the lowest peptide concentration (C = 50 mg/mL), FF peptides predominantly assemble into vesicle-like structures. At C = 85 mg/mL, nanotube and bilayer structures start to form. At C = 120 mg/mL, the three families of structures are almost equally sampled. At the highest peptide concentration (C = 155 mg/mL), the vesicle-like structure disappears and the peptides have a preference to adopt a planar 2D bilayer. These data indicate that FF peptides have a propensity to

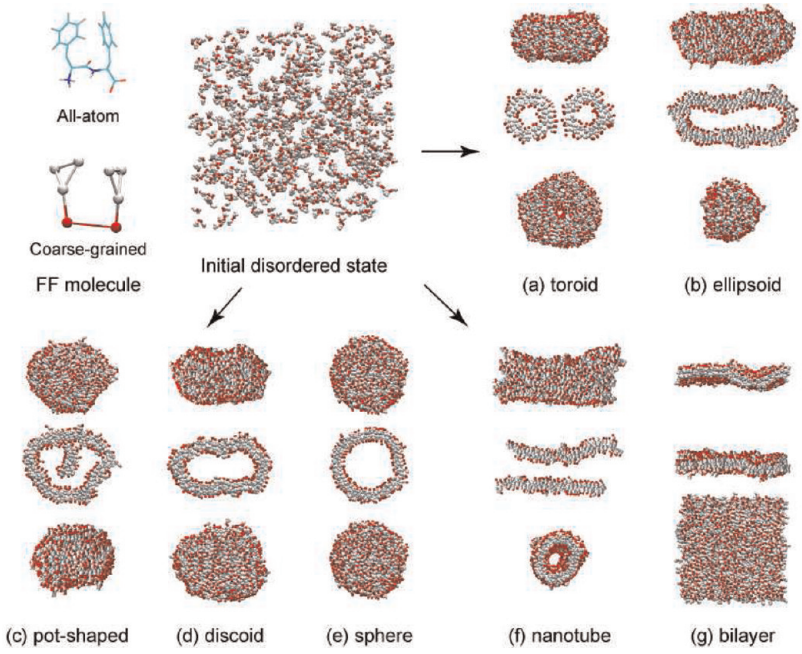

Figure 1. Initial disordered state and seven representative well-organized FF dipeptide assemblies generated in our MD simulations. For each nanostructure, we show a side view (top row), a cross-sectional view through its center of mass and the axis parallel to its principal axis (middle row), and a top view (bottom row). The main-chain beads are in red, and the side-chain beads are in white. There are three families of structures: vesicles with different shapes: (a) toroid, (b) ellipsoid, (c) pot-shaped, (d) discoid, and (e) spherical vesicles; nanotube (f); and bilayer (g). For clarity, a close-up of one FF dipeptide together with its atomistic structure is shown in the top-left corner. In the atomistic structure, carbon atoms are in cyan, oxygen atoms in red, hydrogen atom in white, and nitrogen atom in blue.

form vesicle-like structures at low peptide concentrations and nanotubes at high peptide concentrations, consistent with previous experimental observations that the transformation of nanotubes into vesicles takes place when diluting the D-Phe-D-Phe and the cationic FF nanotube solution.[21,25,26]

Seven representative ordered nanostructures are shown in Figure 1 in the order of their formation concentration from low to high. From all the structures, we find that the FF dipeptide behaves somewhat like a surfactant and the polar main chain groups are isolated from the hydrophobic aromatic groups to form open or closed bilayered structures. The toroid, ellipsoid, pot-shaped, and discoid vesicles in Figure 1a–d are observed in MD trajectories at C = 50 mg/mL. The spherical vesicles and nanotubes in Figure 1e and f are found at C = 85 and 120 mg/mL. The planar 2D bilayer in Figure 1g is obtained only at C = 155 mg/mL. In addition, 1D infinitely long bilayers and 2D flat bilayers with a hole are observed respectively at 85 and 120 mg/mL (data not shown). It should be noted that the formation of vesicles and nanotube-like structure was also observed in the self-assembly of lipids by coarse-grained MD simulations.[34,35] Although the FF nanostructures are reminiscent of nanovesicles and nanotubes formed by lipids, there are important and significant differences in their physical driving forces and formation mechanisms. Unlike lipids, the self-assembly of FF peptides involves both interpeptide main-chain hydrogen-bonding and aromatic side-chain packing. Furthermore, the role of water in the formation of vesicles and nanotubes has not been well studied.

To characterize the well-defined nanostructures, we have calculated their sizes as well as the number of peptide chains in their inner and outer leaflets. The diameter of the spherical vesicle is about 9.2 nm at C = 85 and 120 mg/mL, much smaller than that of the D-Phe-D-Phe vesicle (with a diameter of 200–600 nm),[21] but similar to that of the smallest diphenylglycine spheres (with a diameter of 10–100 nm).[27] As described below, the formation of vesicles and nanotubes involves vesicle fusion. It is conceivable that ongoing fusion events would also lead to larger vesicles in our simulations if the simulations would run long enough. This spherical vesicle consists of 236 peptides in the inner leaflet and 364 peptides in the outer leaflet. The cavity of the spherical vesicle contains 687 water beads. The diameter of the nanotube varies with peptide concentration from 85 to 155 mg/mL, ranging from ~5.1 to ~5.6 nm, which is in the range of FF nanotube sizes observed experimentally (0 < diameter ≤300 nm).[6,22] The nanotube formed at C = 85 mg/mL consists of 230 peptides in the inner leaflet and 370 peptides in the outer leaflet, filled with 271 water beads inside the hollow tube. The flat 2D bilayer formed at C = 155 mg/mL has a thickness of ~1.6 nm and an area of ~160 nm^2.

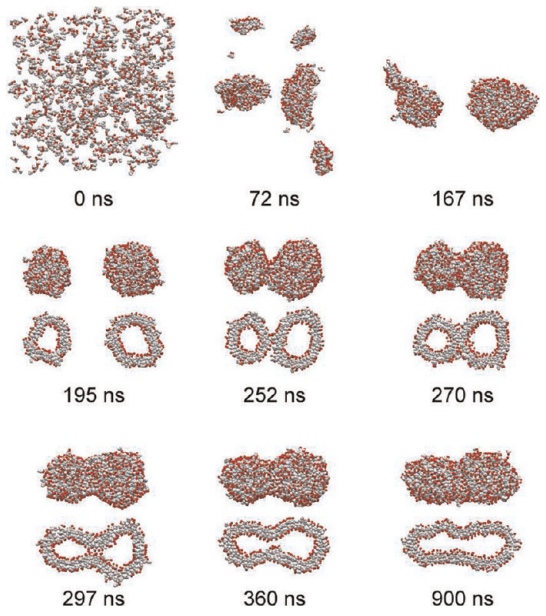

Figure 2. Assembly process of an ellipsoid vesicle through vesicle fusion at the lowest peptide concentration of 50 mg/mL. For each vesicle-like structure, we show a side view and a cross-sectional view through its center of mass and the axis parallel to its principal axis.

It is of particular interest to dissect the assembly pathways leading to nanovesicles and nanotubes. This can be done by probing the structures of the FF assemblies generated in the MD trajectories at different time points at each peptide concentration. At C = 50 mg/mL, we find that the self-assembly of vesicles often involves vesicle fusion, which includes the fusion of two vesicles or the fusion of a vesicle with a bilayer. Fusion events are observed in all of the 10 MD trajectories. One representative assembly pathway of FF peptides into a nanovesicle is shown in Figure 2. Starting from a random conformation, FF peptides form two bilayers with several small clusters (with peptides randomly oriented) within tens of nanoseconds (see the snapshot at t = 72 ns). Then the small clusters merge into the two bilayers, and the bilayers start to bend. A curved bilayer and a vesicle are observed at t = 167 ns. This is followed by the closure of the bilayer to adopt a vesicle-like structure. The two small vesicles both rearrange into a spherical shape around t = 195 ns in order to reduce their solvent exposure. They remain intact until they come into contact with each other at t = 252 ns, from which the fusion process starts. At the first stage of the fusion, the hydrophilic main chains of the outer leaflets of the two small vesicles interact with each other and rearrange into a hemifused intermediate at t = 270 ns. After that, the inner leaflet starts to fuse and a budded vesicle with a neck forms at t = 297 ns. The budded vesicle exists only for several tens of nanoseconds. Then the main-chain groups of the peptides at the neck region begin to separate from each other, and a pear-shaped vesicle forms at t = 360 ns. This vesicle is a metastable state, and it transforms to an ellipsoid vesicle at t = 600 ns (snapshot not shown). This ellipsoid vesicle remains until the end of the simulation (t = 900 ns). The detailed dynamic formation process of the ellipsoid vesicle is shown in a movie in the Supporting Information. We find that the pear-shaped vesicle is an essential intermediate in the assembly pathway leading to the ellipsoid vesicle. The formation process of an ellipsoid vesicle that involves more than two fusion events follows a similar assembly mechanism (see Figure S1 in the Supporting Information).

Fusion events that involve the fusion of a vesicle with a bilayer are also observed at a peptide concentration of 50 mg/mL. Compared to the fusion process of two vesicles into an ellipsoid vesicle in Figure 2, the fusion scenario of a vesicle with a bilayer is rather complex. In addition to the formation of ellipsoid vesicles, it also leads to other shaped vesicle-like structures, including the toroid, pot-shaped, and discoid vesicles. For example, the self-assembly of the toroid vesicle (see Figure S2) involves the fusion of a small bilayer with a large vesicle. Starting from a random configuration, FF peptides assemble into a large bilayer surrounded by small bilayers/clusters at 60 ns. At t = 99 ns, the large bilayer rolls up to form a spherical vesicle, V1, and a small bilayer, B1, fuses with V1. At t = 120 ns, another small bilayer, B2, starts to fuse with another large vesicle, V2. A partially fused intermediate (V2,B2) forms at t = 144 ns, interacting with the first partially fused state (V1,B1). The two partially fused vesicles start to fuse at t = 180 ns and gradually merge into a toroid vesicle. The self-assemblies of discoid and pot-shaped vesicles follow a similar fusion process to the toroid vesicle.

At C = 85 mg/mL, FF dipeptides can spontaneously assemble into vesicles, nanotubes, or bilayers. The formation process of these ordered nanostructures involves either vesicle fusion or no vesicle fusion. Fusion events are observed in six out of ten MD runs, and four (two) out of the six runs lead to ellipsoid vesicles (tubes). A representative self-assembly pathway of a FF nanotube is shown in Figure 3. Starting from a random configuration, FF peptides assemble into three bilayers within tens of nanoseconds (see the snapshot at t = 60 ns). This is followed by the formation of a spherical vesicle and an ellipsoid vesicle through bilayer closure and vesicle fusion (see the snapshot at t = 100 ns). From t = 144 to 540 ns, a vesicle fusion process, similar to that occurring at C = 50 mg/mL (see Figure 2), is observed. At t = 540 ns, an ellipsoidal vesicle forms *via* the fusion of two small vesicles. Remarkably, the formation of the ellipsoid vesicle makes the concentration of FF dipeptides increase along the long axis of the vesicle. This allows FF peptides near the end of the primary cell to have interactions with nearby FF peptides in neighboring

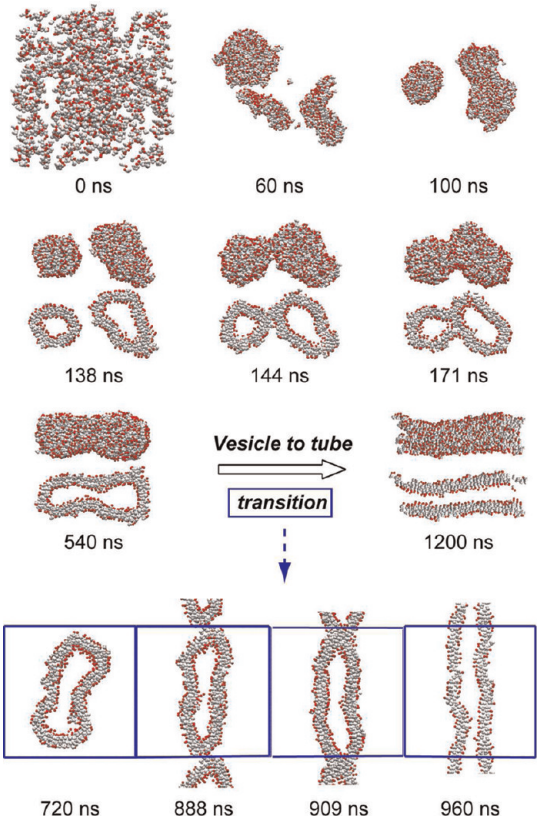

Figure 3. Assembly process of nanotube through vesicle fusion at a relatively high peptide concentration of 85 mg/mL. For each vesicle-like or tubular structure, we show a side view and/or a cross-sectional view through its center of mass and the axis parallel to its principal axis. In order to show the concentration-induced vesicle-to-tube transition process, a simulation box is displayed for the snapshots from t = 720 to 960 ns.

image cells that are similar to the interactions between FF peptides in the primary cell. At t = 888 ns, the vesicle in the primary cell starts to fuse with the vesicles in its two neighboring image cells. A shape transformation from the vesicle to the nanotube takes place at t = 960 ns. This is followed by the fine rearrangement of the FF peptides, and a well-organized nanotube forms at t = 1200 ns. Compared with the formation of the vesicle-like structure at C = 50 mg/mL, the structure transition from vesicles to nanotubes observed at C = 85 mg/mL likely results from the increased peptide concentration. Our result is consistent with recent experimental observations that a spontaneous transformation of vesicles into nanotubes takes place by concentrating the cationic FF peptide vesicle solution.[25,26]

The self-assembly pathway of FF peptides at a higher peptide concentration becomes simpler, during which the fusion event occurs very rarely. This can be seen in the assembly process of FF peptides at C = 120 mg/mL. Two representative pathways, which lead to a spherical vesicle and a nanotube respectively, are given in Figure 4. Starting from a random state, the peptides form clusters first and then assemble into a bilayer in several tens of nanoseconds (see the snapshot at t = 42 ns in trajectory A). Then the bilayer bends in three dimensions and adopts a hemispherical shape at t = 72 ns. It closes rapidly and forms a spherical vesicle at t = 108 ns. The vesicle remains until the end of the MD simulation (t = 900 ns). Similar to the self-assembly pathway of the spherical vesicle shown in trajectory A, the formation process of the nanotube is also accompanied by a rapid formation of a bilayer (see the snapshot at t = 90 ns). However the bilayer bends in two dimensions (t = 180 ns) and gradually forms a tubular structure (see the snapshot at 900 ns). It is noted that bilayers are observed as an intermediate state prior to the formation of vesicle-like and tubular structures under all peptide concentrations. At the highest peptide concentration studied in this work, FF peptides rarely assemble into tubular structures, while they have a strong preference to adopt a planar 2D bilayer (see Table 1 and Figure 1g).

We also use the Minkowski functionals to monitor the topology change of FF assembly quantitatively throughout the simulation, as done previously by Marrink and Mark in studying the formation of lipid vesicles.[34] For a three-dimensional system, there are four independent Minkowski functionals: the volume V, the surface area S, the Euler characteristic χ, and the mean curvature H of the surface. The volume is not sensitive to the change of topology and remains essentially constant during the simulation due to the very small compressibility of the peptides. Therefore, we calculate the other three measures using the procedure of Hyde *et al.*[36] As an example, we present in Figure S4 the time evolution of the three measures for the formation of a spherical vesicle at C = 120 mg/mL (corresponding to trajectory A in Figure 4). It can be seen from Figure S4 that the surface area and the mean curvature decrease rapidly within the first 25 ns, indicating the formation of multiple unconnected small clusters. The corresponding Euler number is larger than 2 because each cluster contributes an Euler characteristic of 2 or 1 depending on the shape of the small cluster. After that, the three parameters continue to decrease with time and χ reaches 1 at t = 27 ns, at which one large bilayer forms. This is followed by a slow decrease of surface area and curvature in the next 50 ns, while χ remains at 1. Within this time period, the bilayer bends and forms a curved bilayer. At t = 95 ns, the Euler number increases to 2 and the surface area reaches a minimum value of 580 nm^2, when the bilayer becomes closed and turns into a vesicle. At this time point, the mean curvature reaches 0.22 nm^{-1}, which is equal to the reciprocal of the outer radius (4.5 nm) of the vesicle. After that, the vesicle remains stable and the surface area S, the Euler characteristic χ, and the mean curvature H of the surface all remain invariant.

To further understand the self-assembly pathways of FF peptides into nanovesicles and nanotubes at

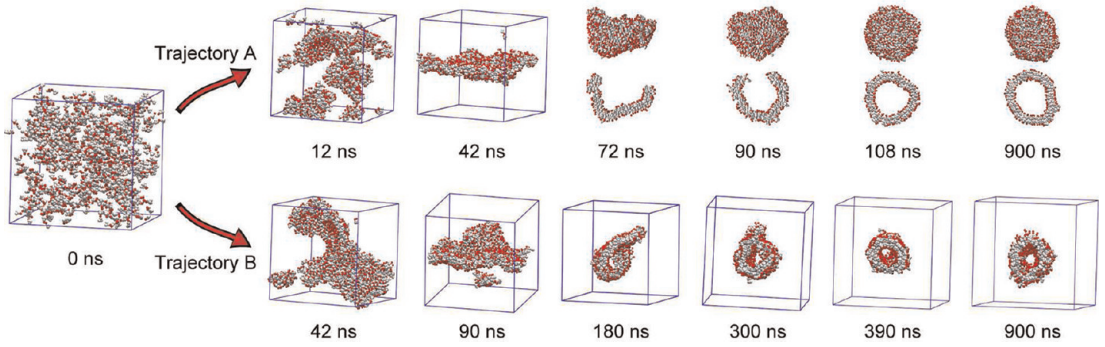

Figure 4. Assembly process of spherical vesicle (trajectory A) and nanotube (trajectory B) without involving vesicle fusion at a peptide concentration of 120 mg/mL. In trajectory A, in order to clearly show the process of vesicle formation, we give a side view and a cross-sectional view without the simulation box.

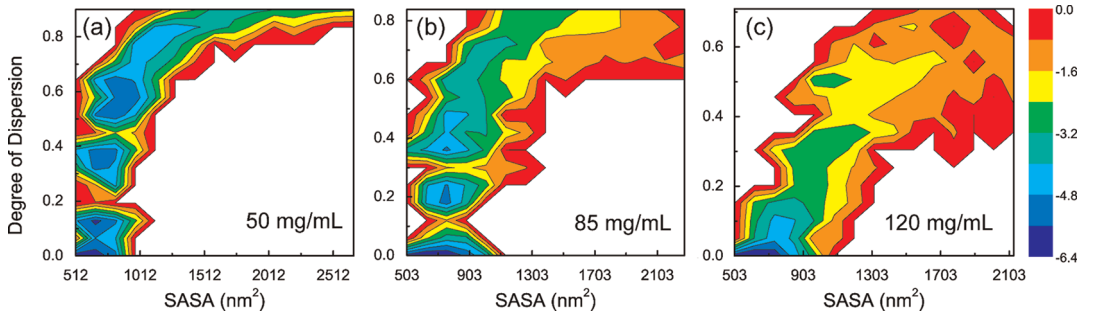

Figure 5. Self-assembly free energy landscape of FF peptides at three different concentrations projected on the solvent-accessible surface area and the dispersion degree of peptides. The unit of free energy is kcal/mol.

different peptide concentrations, we construct the free energy landscape for C = 50, 85, and 120 mg/mL in Figure 5. The free energy landscape is projected onto the two reaction coordinates described in the Methods section: the solvent accessible surface area (SASA) and the dispersion degree of FF peptides (D_{disp}). As seen in Figure 5, the free energy landscape is very rugged at C = 50 mg/mL and there are three minimum-energy basins separated by energy barriers. The three basins are located at (SASA, D_{disp}) values of (974 nm^2, 0.55), (820 nm^2, 0.35), and (743 nm^2, 0.1), corresponding to respectively multiple small vesicles and/or bilayers, two vesicles, and one partially or completely fused vesicle. It can be seen from Figure 5a that once the peptides aggregate together, the SASA decreases sharply, whereas the dispersion degree of the peptides is still larger than 0.5 (indicating that the largest assembly consists of less than 300 FF peptides). When the SASA reaches 820 nm^2 and the D_{disp} drops to ~0.35, two vesicles form and a fusion process starts. Once the two vesicles merge into one large vesicle, the D_{disp} approaches zero (in some cases, there are still some peptides isolated from the ordered nanostructure, so D_{disp} might not be exactly zero, but a small number between 0 and 0.1). The SASA difference between different shapes of vesicles is so small that we fail to separate them in the free energy landscape with a reasonable resolution. At C = 85 mg/mL, although there are also three minimum-energy basins in the free energy landscape (see Figure 5b), the free energy landscape becomes smoother than that at C = 50 mg/mL. In particular, the first basin (from top to bottom), located at (SASA, D_{disp}) values of (819 nm^2, 0.35), becomes very shallow. It corresponds to two unfused vesicles. This indicates that at C = 85 mg/mL it is much easier for small FF clusters/vesicles to assemble into two larger vesicles than at C = 50 mg/mL. The middle and the bottom energy basins, located at (SASA, D_{disp}) values of (810 nm^2, 0.2) and (692 nm^2, 0.0), correspond respectively to one partially fused vesicle and one completely fused vesicle/nanotube. At C = 120 mg/mL, there is only one free energy basin located at (SASA, D_{disp}) values of (676 nm^2, 0.0), and the free energy landscape becomes funnel-like. These results demonstrate that the complexity of the free energy landscape and the assembly pathway are strongly related to the FF peptide concentrations. The results from our simulation would provide useful molecular insights into the self-assembly mechanism of FF-based nanovesicles/nanotubes, although the peptide concentration used in this study is much higher than that used experimentally. On the basis of the increased complexity of the free energy landscape with the decrease of peptide concentration found here, we propose that the formation of experimentally observed FF-based nanostructures occurs through multiple fusion events.

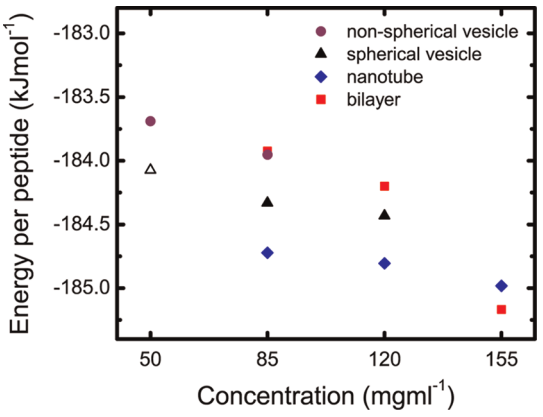

Figure 6. Total potential energy (per peptide) of well-organized FF nanostructures formed at four different peptide concentrations. The well-organized nanostructures include nonspherical vesicles, spherical vesicles, nanotubes, and bilayers. The nonspherical vesicles include ellipsoid, toroid, discoil, and pot-shaped vesicles. The bilayer at *C* = 85 mg/mL is a 1D infinitely long bilayer, the bilayer at *C* = 120 mg/mL is a 2D infinitely large bilayer with a hole in its center, and the bilayer at *C* = 155 mg/mL is a flat 2D infinite bilayer. In the energy calculation, the data in the first 600 ns of each simulation are discarded, and the data in the first 300 ns are discarded for *C* = 155 mg/mL.

Having investigated the assembly pathway of FF dipeptides into nanostructures at different peptide concentrations, we then reveal the physical driving forces underlying the different nanostructure formation. To this end, we first examine the relative stabilities of different nanostructures at each peptide concentration by calculating the total potential energy (including the solvation effect as described in the Methods section). It can be seen from Figure 6 that at *C* = 50 mg/mL the potential energy of spherical vesicles (black open triangle) is lower than that of nonspherical vesicles, indicating that the spherical vesicle is more stable than the nonspherical vesicle. The spherical vesicle is obtained from three independent MD runs at *C* = 50 mg/mL starting from a flat 2D bilayer formed at *C* = 155 mg/mL. It is noted that none of the 10 MD runs at *C* = 50 mg/mL starting from a random state leads to a perfectly spherical vesicle within 1800 ns. This is probably due to the short time scale of MD simulations, which is not long enough for the system to transform into the spherical vesicle. For the five different shapes of 3D-closed vesicle-like structures, we can also estimate their relative stabilities by using a quantity, reduced volume, according to the relationship between the reduced volume and free energy reported previously.[37] The reduced volume is given by $V/[(4\pi/3)R_0^3]$, where V is the volume of the vesicle and $R_0 = (A/4\pi)^{1/2}$ is the radius of a sphere with the same surface area as the vesicle. The reduced volumes of the toroid, ellipsoid, pot-shaped, discoid, and spherical vesicles are 0.775, 0.821, 0.878, 0.908, and 1.0, respectively. The larger the reduced volume is, the more stable the vesicle-like structure becomes.[37] Therefore, the spherical vesicle is the most stable one among the five different shapes of vesicles. The nonspherical vesicle might be a trapped assembly or an intermediate state on the pathway leading to spherical vesicles, depending on the peptide concentration and/or preparation procedures.

At *C* = 85 and 120 mg/mL, nanotubes have the lowest potential energy, spherical vesicles the second lowest, and nonspherical vesicles or bilayers the highest. This indicates that under these two peptide concentrations it is most energetically favorable for FF dipeptides to adopt tubular structures but less favorable to form vesicles and bilayers. This result provides an explanation for the existing experimental observations that FF or D-Phe-D-Phe dipeptides often self-assemble into nanotubes,[6,18−20] while rarely form vesicles.[21] At *C* = 155 mg/mL, the potential energy of the flat bilayer is slightly lower than that of the nanotube, suggesting that the flat bilayer is marginally favored over the nanotube. To the best of our knowledge this is the first report of bilayer formation by FF dipeptides. Interestingly, the formation of flat bilayers is also reported in recent experimental studies for both KLVFFAL and AAAAAAK peptides.[38,39] On the basis of our results, we propose that FF dipeptides can self-organize into nanotubes, spherical vesicles, or bilayers by fine-tuning peptide concentrations.

We then determine the major contribution to the total potential energy of FF nanostructures. This is done by calculating the probability distribution of the different energy components: the protein−protein electrostatic interactions (*i.e.*, between main-chain and main-chain), the protein−protein (Prot−Prot) vdW interactions (including both main-chain−main-chain and side-chain−side-chain interactions), the protein−water (Prot−Sol) interactions, and the cavity hydration energy. Figure 7 shows that the contribution of the protein−protein electrostatic energy (Prot−Prot: E_{elec}) to the total energy for different structures is quite similar, as the energies are all distributed in a very narrow region (−2.6 to −3.2 kJ/mol) and the distribution peaks are all centered at −2.9 kJ/mol under the four peptide concentrations. Therefore, the total energy difference between different nanostructures predominantly comes from the other three terms: the Prot−Prot vdW interactions, the Prot−Sol interactions, and the cavity hydration energy. Under each peptide concentration, the three energy terms contribute differently to the total energy for vesicles, tubes, and bilayers. At *C* = 50 and 85 mg/mL, the Prot−Prot vdW interaction in nonspherical vesicles is stronger than that in spherical vesicles due to a closer packing of FF peptides in nonspherical vesicles. However, the Prot−Sol interaction (which can prevent peptide dissociation) in nonspherical vesicles becomes much weaker because the cavity of nonspherical vesicles is filled with fewer water beads than that of spherical vesicles. The cavity hydration

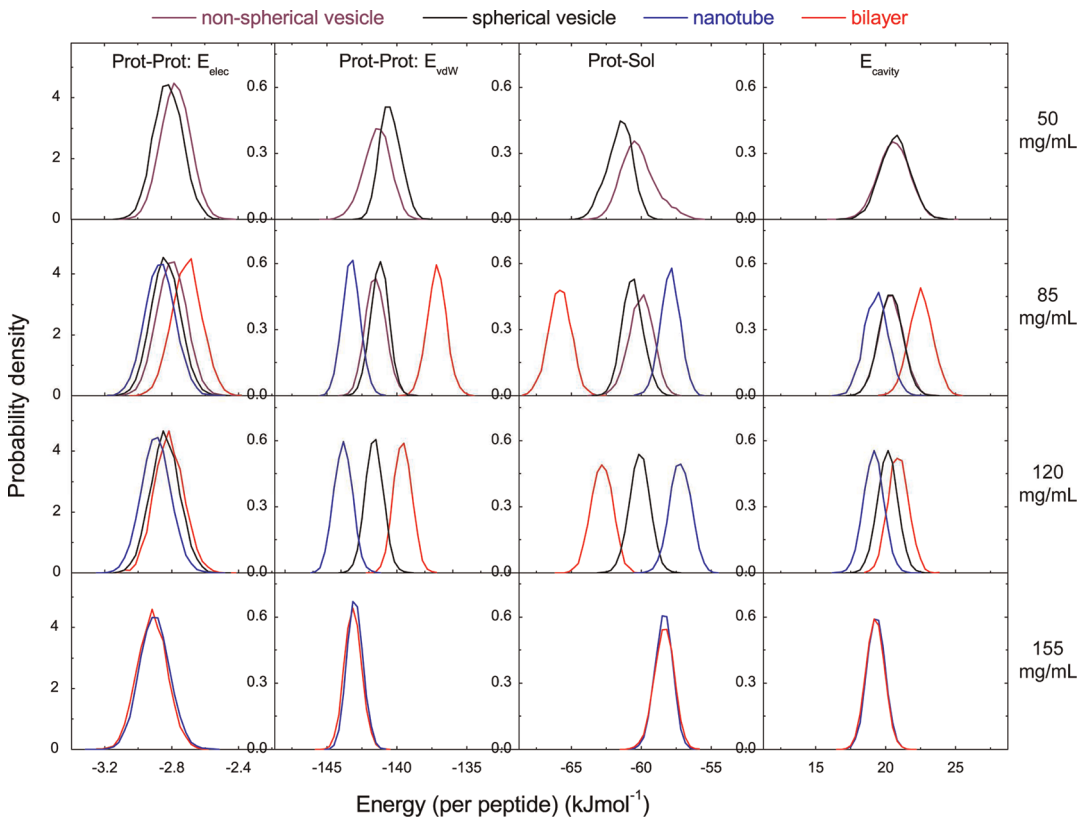

Figure 7. Probability distribution of the total potential energy components of well-organized FF nanostructures formed at four different peptide concentrations. The energy components include protein−protein electrostatic (Prot−Prot: E_{elec}), protein−protein van der Waals (Prot−Prot: E_{vdW}), protein−water (Prot−Sol), and cavity hydration energy (E_{cavity}). The data used here are the same as those used in Figure 6.

energy is quite similar for spherical and nonspherical vesicles. Thus the total energy gained by forming a nonspherical vesicle containing closer packing of FF peptides is overwhelmed by an increase in Prot−Sol interactions in spherical vesicles, which leads to the spherical vesicle being more energetically favorable. This result suggests that water molecules play a significant role in mediating the formation of different shapes of vesicles at low peptide concentrations. At higher peptide concentrations (C = 85 and 120 mg/mL), the competition among the Prot−Prot, the Prot−Sol, and the cavity hydration energy terms becomes more complicated, as they contribute differently to the formation of vesicles, tubes, and bilayers (see Figure 7). Ranking the nanostructures by Prot−Prot interaction strength from the strongest to the weakest, the nanotube is first, the vesicle is second, and the long narrow 1D bilayer or the bilayer with a hole is last. This ranking can be understood by the different extents of close packing of FF peptides in different nanostructures. The closer the packing is, the stronger the Prot−Prot interaction becomes. As nanotubes are closed in 2D and vesicles in 3D, the packing of FF peptides in nanotubes is closer than that in vesicles. Because molecular interaction pairs in the infinitely long 1D bilayer or in the 2D bilayer with a hole are smaller than those in vesicles and tubes, the Prot−Prot interaction in bilayers is the weakest among the different nanostructures. The strengthening in the Prot−Prot interaction weakens the Prot−Sol interaction and leads to more free water beads in the bulk (corresponding to a decrease of the cavity hydration energy). These three different interactions cooperatively modulate the formation and the relative stabilities of different nanostructures. At the highest peptide concentration (C = 155 mg/mL), the packing of FF peptides in a 2D infinitely large bilayer is closer than that in tubular structures, leading to a slightly stronger Prot−Prot interaction in bilayers. The differences in the Prot−Sol interaction energy and in the cavity hydration energy are quite small for the two structures. Therefore the formation of FF bilayers and nanotubes at C = 155 mg/mL is mostly governed by the Prot−Prot interaction. These results demonstrate that the self-organization of FF dipeptides into different ordered nanostructures at different peptide concentrations is modulated by a delicate balance of the protein−protein interaction and the protein−water interaction (including the cavity hydration energy).

It has been proposed that the FF-based nanostructures are stabilized by a combination of aromatic stacking and hydrogen bonding.[6,20] However, there is no direct evidence showing this. In this context, we first

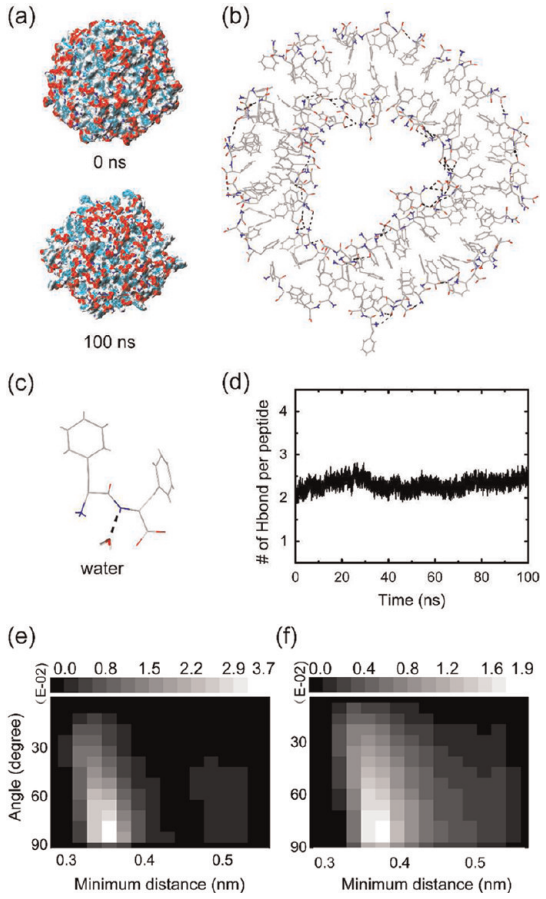

Figure 8. Simulation results from an all-atom MD run starting from our reconstructed atomistic structure of a FF spherical vesicle from CG beads. (a) Initial and final states, where main-chain O atoms are in red, N atoms are in blue, and side-chain atoms are in cyan. (b) Cross section, where side-chain atoms are in gray, main-chain N atoms are in blue, and main-chain O atoms are in red; head-to-tail peptide hydrogen bonds are shown with a black dashed line. (c) FF monomer from (b), with a peptide−water hydrogen bond represented by a black dashed line. Probability distribution of (e) intrapeptide and (f) interpeptide aromatic ring angles as a function of the minimum distance between two rings. The probability is largest at 90°. In the calculation, all the intramolecular pairs are considered, while the intermolecular pairs are considered if their minimum distance is less than 0.56 nm.

calculate the intrapeptide aromatic ring angle and the interpeptide aromatic ring angle using the CG model.[32] Our calculation shows that the two types of angles are both distributed mainly in the range 30−90°, with almost equal population for each angle in this range. Similar results are obtained for both vesicles and nanotubes. This result suggests aromatic stacking is important in stabilizing ordered FF nanoarchitectures. To further examine the crucial role of aromatic stacking on the nanostructure formation, we have carried out three independent 400 ns control MD simulations on 600 LF dipeptides under C = 85 mg/mL starting from a random configuration. However, none of the three ordered FF nanostructures (including vesicles, tubes, and bilayers) are observed in the three MD runs (see Figure S3).

In the CG model,[32] the "ring" structure of Phe cannot represent the aromatic phenol group accurately (the phenol group is represented by three beads, and the C_β atom is omitted), and hydrogen bonds are not explicitly described (there is only one bead for the main chain). Therefore, we use the modified version of GROMACS-3.3.1[40] with the Gromos96 43a1 force field[41] to generate a fine-grained structure of a spherical vesicle generated in the CG MD trajectories. To save computational time, we take a small vesicle (consisting of 199 FF peptides) to simulate. We perform a 100 ns all-atom MD simulation at a temperature of 310 K and a pressure of 1 bar starting from our reconstructed model (Figure 8a). Simulation details are given in the Supporting Information. The total number of atoms (including water molecules and FF peptides) in the all-atom system is 48 478. The total, hydrophobic, and hydrophilic SASAs of the vesicle do not change much during the full period of MD simulation, indicating that this reconstructed all-atom model is stable within the 100 ns MD simulation (Figure S4a). The simulated vesicle at t = 100 ns is given in Figure 8a. A cross section of the final structure and a single FF peptide from the cross section are shown respectively in Figure 8b and c. We observe the formation of interpeptide head (NH_3^+) to tail (COO^-) hydrogen bonds by consecutive peptides (see Figure 8b) and the adoption of T-shaped aromatic stacking within FF monomers (see Figure 8c). It is noted that the two aromatic rings stay at the same side of the peptide bond (see Figure 8c and Figure S4b). These structural features are similar to those in the FF crystals.[17] Our analysis using the 100 ns data shows that there are ∼2.5 interpeptide hydrogen bonds per peptide (Figure 8d). Two out of ∼2.5 hydrogen bonds are interpeptide head-to-tail hydrogen bonds (Figure 8b), and the remaining 0.5 hydrogen bonds are formed by the FF main-chain atoms with water molecules (Figure 8c). Calculation of the intrapeptide aromatic ring angle shows that the intrapeptide aromatic ring angle is mostly distributed in the range 60−90°, with a high probability around 90° at a minimum distance of ∼0.35 nm (Figure 8e). The deviation of this angle from 90° implies that the two aromatic rings have a certain freedom to move at physiological temperature due to thermal fluctuations. The distribution of the interpeptide aromatic ring angle displays a similar feature (see Figure 8f), having a high probability at a minimum distance of ∼0.37 nm, implying that the two rings have a strong preference to be orthogonally aligned. These data provide evidence that FF-based nanovesicles are stabilized by a combination of T-shaped aromatic stacking, interpeptide head-to-tail hydrogen bonds, and peptide−water hydrogen bonds.

CONCLUSIONS

By using large-scale CG MD simulations, we have studied the assembly process of FF peptides at different peptide concentrations. We find that FF peptides can spontaneously assemble into spherical vesicles and tubes, as well as other new ordered nanostructures including toroid, ellipsoid, discoid, and pot-shaped vesicles depending on the peptide concentration. A combination of intra- and inter-peptide T-shaped aromatic stacking, interpeptide head-to-tail hydrogen bonding, and peptide–water hydrogen bonding is found to be important in stabilizing the ordered nanostructures. The assembly pathways are concentration-dependent. At low peptide concentrations, the self-assembly of FF-based nanotubes/nanovesicles involves the fusion of small vesicles and/or bilayers, whereas at high concentrations, it occurs through the formation of a bilayer first, followed by the bending and the closure of the bilayer. The calculated free energy landscapes at three different peptide concentrations display different features: the lower the peptide concentration is, the more rugged the free energy landscape becomes.

Based on the increased complexity of the free energy landscape with the decrease of peptide concentration, we propose that the experimentally observed FF-based nanostructures might come through the following steps: (i) formation of small clusters, followed by the growth of small clusters into bilayers; (ii) curving and closure of bilayer into vesicles; (iii) formation of several tens to hundreds of nanometers vesicle-like or tubular nanostructures *via* vesicle fusion. Energetic and structural analyses suggest that the formation of different shapes of nanostructures is a result of the delicate balance between peptide–peptide and peptide–water interactions, and the aromatic stacking interaction is the dominant driving force for the self-organization. Collectively, our findings provide theoretical insights into peptide nanostructure formation and would be helpful for designing a variety of versatile peptide nanostructures with unique properties.

METHODS

Coarse-Grained MD Simulation. Molecular dynamics simulations have been widely used in the conformational studies of biomolecules.[42−48] In this work, we use the recently developed CG MARTINI V2.1 force field to model the FF dipeptides and water molecules[32,33] to save computational cost, as mentioned earlier. In this force field, a phenylalanine molecule is represented by four beads, one bead for the main chain and three beads for the side-chain ring structure. The N-terminal main-chain bead of FF has one positive charge, and the C-terminal main-chain bead has one negative charge. Four water molecules are mapped onto one bead with no charge. This force field allows a 4-fold reduction in the number of particles represented and a 10−30-fold increase in the time step size in MD, as compared with united-atom simulations.[33]

We have performed 40 MD simulations on a system consisting of 600 FF peptides at four different peptide concentrations: 50, 85, 120, and 155 mg/mL. The peptide concentration in experimental studies is a few mg/mL, much lower than the concentration used in our simulation. As simulating the assembly process of peptides starting from a random state at low peptide concentration is very time-consuming, we applied the strategy of using high peptide concentrations to reduce computational cost, which is often used computationally.[34,49,50] At each concentration, 10 MD runs have been performed using different initial velocities starting from a random configuration with each peptide chain randomly oriented. The simulation time for each MD run is 0.9−1.8 μs at 50 mg/mL, 1.2 μs at 85 mg/mL, 0.9 μs at 120 mg/mL, and 0.6 μs at 155 mg/mL. All MD simulations have been carried out in the NPT ensemble with GROMACS software[51] using a time step of 30 fs.[52] The system is weakly coupled to external temperature and pressure baths using the Berendsen coupling methods.[53] A temperature of 310 K is kept with a coupling constant of 0.3 ps, and a pressure of 1 atm is maintained with a coupling constant of 3 ps. Electrostatic and van der Waals (vdW) interactions are used in their shifted forms with a cutoff at a distance of 1.2 nm. The vdW potential is shifted from 0.9 to 1.2 nm, and the electrostatic potential is shifted from 0.0 to 1.2 nm.[32] The neighbor list is updated every 10 steps with a cutoff distance of 1.2 nm.

Analysis. Analysis is performed using our in-house-developed codes and the GROMACS facilities. To follow the assembly process and characterize the dominant structures of FF assemblies, we monitor the conformations at different time points in representative MD trajectories as well as the self-assembly free energy landscapes at three different peptide concentrations. The free energy landscapes are constructed using $-RT \log P(x,y)$, where $P(x,y)$ is the probability (from histogramming) of the particular conformation along two preselected reaction coordinates x and y. In this study, these two reaction coordinates are the solvent-accessible surface area and the degree of dispersion of the peptides. The latter is obtained by $D_{disp} = 1 - n_{max}/N$, where n_{max} is the maximum number of FF peptide chains in a single assembled cluster (the largest cluster) and N is the total number (600) of FF peptides in the system. Two peptide chains are considered to form a cluster if their minimum distance is less than 0.65 nm. A peptide chain is considered to join to a preformed cluster if the minimum distance between this chain and any chain in the preformed cluster is less than 0.65 nm. To understand the physical driving forces underlying the formation of different types of FF nanostructures, we calculate their total potential energies by including the solvation effect and the probability distribution of different energy terms. The solvation energy consists of protein–water electrostatic energy, protein–water vdW dispersion energy, and cavity hydration energy (due to excluded volume effects).[54] As the partial charge of water beads is zero in the CG model, the protein–water electrostatic energy term vanishes in the calculation. The interplanar angle between two aromatic rings is calculated by the angle between the surface normals of the two rings. The number of interpeptide hydrogen bonds is also calculated. A hydrogen bond is counted if the N···O distance is less than 0.35 nm and the N–H···O angle is greater than 150°. All the snapshots are drawn using the VMD software.[55]

Conflict of Interest: The authors declare no competing financial interest.

Acknowledgment. G.W. acknowledges the support from the NSF of China (grant no. 11074047) and Research Fund for the Doctoral Program of Higher Education of China (20100071110006). R.Z. acknowledges the support from the IBM Blue Gene Science

program. We would also like to acknowledge the support from the 111 Project (B06011). Simulations were performed at the Shanghai Supercomputing Center and the National High Performance Computing Center of Fudan University.

Supporting Information Available: This material is available free of charge *via* the Internet at http://pubs.acs.org.

REFERENCES AND NOTES

1. Cherny, I.; Gazit, E. Amyloids: Not Only Pathological Agents but Also Ordered Nanomaterials. *Angew. Chem., Int. Ed.* **2008**, *47*, 4062–4069.
2. Gazit, E. Self-Assembled Peptide Nanostructures: The Design of Molecular Building Blocks and Their Technological Utilization. *Chem. Soc. Rev.* **2007**, *36*, 1263–1269.
3. Zhao, X. B.; Pan, F.; Xu, H.; Yaseen, M.; Shan, H. H.; Hauser, C. A. E.; Zhang, S. G.; Lu, J. R. Molecular Self-Assembly and Applications of Designer Peptide Amphiphiles. *Chem. Soc. Rev.* **2010**, *39*, 3480–3498.
4. Liu, L.; Busuttil, K.; Zhang, S.; Yang, Y. L.; Wang, C.; Besenbacher, F.; Dong, M. D. The Role of Self-Assembling Polypeptides in Building Nanomaterials. *Phys. Chem. Chem. Phys.* **2011**, *13*, 17435–17444.
5. Ghadiri, M. R.; Granja, J. R.; Milligan, R. A.; Mcree, D. E.; Khazanovich, N. Self-Assembling Organic Nanotubes Based on a Cyclic Peptide Architecture. *Nature* **1993**, *366*, 324–327.
6. Reches, M.; Gazit, E. Casting Metal Nanowires within Discrete Self-Assembled Peptide Nanotubes. *Science* **2003**, *300*, 625–627.
7. Aggeli, A.; Nyrkova, I. A.; Bell, M.; Harding, R.; Carrick, L.; McLeish, T. C. B.; Semenov, A. N.; Boden, N. Hierarchical Self-Assembly of Chiral Rod-Like Molecules as a Model for Peptide Beta-Sheet Tapes, Ribbons, Fibrils, and Fibers. *Proc. Natl. Acad. Sci. U. S. A.* **2001**, *98*, 11857–11862.
8. Vauthey, S.; Santoso, S.; Gong, H. Y.; Watson, N.; Zhang, S. G. Molecular Self-Assembly of Surfactant-Like Peptides to Form Nanotubes and Nanovesicles. *Proc. Natl. Acad. Sci. U. S. A.* **2002**, *99*, 5355–5360.
9. Lu, K.; Jacob, J.; Thiyagarajan, P.; Conticello, V. P.; Lynn, D. G. Exploiting Amyloid Fibril Lamination for Nanotube Self-Assembly. *J. Am. Chem. Soc.* **2003**, *125*, 6391–6393.
10. Reches, M.; Gazit, E. Controlled Patterning of Aligned Self-Assembled Peptide Nanotubes. *Nat. Nanotechnol.* **2006**, *1*, 195–200.
11. Yan, X. H.; Zhu, P. L.; Li, J. B. Self-Assembly and Application of Diphenylalanine-Based Nanostructures. *Chem. Soc. Rev.* **2010**, *39*, 1877–1890.
12. Biswas, K.; Rao, C. N. R. Nanostructured Peptide Fibrils Formed at the Organic-Aqueous Interface and Their Use as Templates to Prepare Inorganic Nanostructures. *ACS Appl. Mater. Interfaces* **2009**, *1*, 811–815.
13. Han, T. H.; Lee, W. J.; Lee, D. H.; Kim, J. E.; Choi, E. Y.; Kim, S. O. Peptide/Graphene Hybrid Assembly into Core/Shell Nanowires. *Adv. Mater.* **2010**, *22*, 2060–2064.
14. Han, T. H.; Oh, J. K.; Lee, G. J.; Pyun, S. I.; Kim, S. O. Hierarchical Assembly of Diphenylalanine into Dendritic Nanoarchitectures. *Colloids Surf., B* **2010**, *79*, 440–445.
15. Zhu, P. L.; Yan, X. H.; Su, Y.; Yang, Y.; Li, J. B. Solvent-Induced Structural Transition of Self-Assembled Dipeptide: From Organogels to Microcrystals. *Chem.—Eur. J.* **2010**, *16*, 3176–3183.
16. Kim, J.; Han, T. H.; Kim, Y. I.; Park, J. S.; Choi, J.; Churchill, D. C.; Kim, S. O.; Ihee, H. Role of Water in Directing Diphenylalanine Assembly into Nanotubes and Nanowires. *Adv. Mater.* **2010**, *22*, 583–587.
17. Gorbitz, C. H. Nanotube Formation by Hydrophobic Dipeptides. *Chem.—Eur. J.* **2001**, *7*, 5153–5159.
18. Adler-Abramovich, L.; Reches, M.; Sedman, V. L.; Allen, S.; Tendler, S. J. B.; Gazit, E. Thermal and Chemical Stability of Diphenylalanine Peptide Nanotubes: Implications for Nanotechnological Applications. *Langmuir* **2006**, *22*, 1313–1320.
19. Kol, N.; Adler-Abramovich, L.; Barlam, D.; Shneck, R. Z.; Gazit, E.; Rousso, I. Self-Assembled Peptide Nanotubes Are Uniquely Rigid Bioinspired Supramolecular Structures. *Nano Lett.* **2005**, *5*, 1343–1346.
20. Gorbitz, C. H. The Structure of Nanotubes Formed by Diphenylalanine, the Core Recognition Motif of Alzheimer's Beta-Amyloid Polypeptide. *Chem. Commun.* **2006**, 2332–2334.
21. Song, Y. J.; Challa, S. R.; Medforth, C. J.; Qiu, Y.; Watt, R. K.; Pena, D.; Miller, J. E.; van Swol, F.; Shelnutt, J. A. Synthesis of Peptide-Nanotube Platinum-Nanoparticle Composites. *Chem. Commun.* **2004**, 1044–1045.
22. Reches, M.; Gazit, E. Formation of Closed-Cage Nanostructures by Self-Assembly of Aromatic Dipeptides. *Nano Lett.* **2004**, *4*, 581–585.
23. Smith, A. M.; Williams, R. J.; Tang, C.; Coppo, P.; Collins, R. F.; Turner, M. L.; Saiani, A.; Ulijn, R. V. Fmoc-Diphenylalanine Self Assembles to a Hydrogel Via a Novel Architecture Based on Pi-Pi Interlocked Beta-Sheets. *Adv. Mater.* **2008**, *20*, 37–41.
24. Reches, M.; Gazit, E. Self-Assembly of Peptide Nanotubes and Amyloid-Like Structures by Charged-Termini-Capped Diphenylalanine Peptide Analogues. *Isr. J. Chem.* **2005**, *45*, 363–371.
25. Yan, X. H.; He, Q.; Wang, K. W.; Duan, L.; Cui, Y.; Li, J. B. Transition of Cationic Dipeptide Nanotubes into Vesicles and Oligonucleotide Delivery. *Angew. Chem., Int. Ed.* **2007**, *46*, 2431–2434.
26. Yan, X. H.; Cui, Y.; He, Q.; Wang, K. W.; Li, J. B.; Mu, W. H.; Wang, B. L.; Ou-yang, Z. C. Reversible Transitions between Peptide Nanotubes and Vesicle-Like Structures Including Theoretical Modeling Studies. *Chem.—Eur. J.* **2008**, *14*, 5974–5980.
27. Scanlon, S.; Aggeli, A. Self-Assembling Peptide Nanotubes. *Nano Today* **2008**, *3*, 22–30.
28. Flock, D.; Rossetti, G.; Daidone, I.; Amadei, A.; Di Nola, A. Aggregation of Small Peptides Studied by Molecular Dynamics Simulations. *Proteins* **2006**, *65*, 914–921.
29. Tamamis, P.; Adler-Abramovich, L.; Reches, M.; Marshall, K.; Sikorski, P.; Serpell, L.; Gazit, E.; Archontis, G. Self-Assembly of Phenylalanine Oligopeptides: Insights from Experiments and Simulations. *Biophys. J.* **2009**, *96*, 5020–5029.
30. Villa, A.; van der Vegt, N. F. A.; Peter, C. Self-Assembling Dipeptides: Including Solvent Degrees of Freedom in a Coarse-Grained Model. *Phys. Chem. Chem. Phys.* **2009**, *11*, 2068–2076.
31. Villa, A.; Peter, C.; van der Vegt, N. F. A. Self-Assembling Dipeptides: Conformational Sampling in Solvent-Free Coarse-Grained Simulation. *Phys. Chem. Chem. Phys.* **2009**, *11*, 2077–2086.
32. Monticelli, L.; Kandasamy, S. K.; Periole, X.; Larson, R. G.; Tieleman, D. P.; Marrink, S. J. The Martini Coarse-Grained Force Field: Extension to Proteins. *J. Chem. Theory Comput.* **2008**, *4*, 819–834.
33. Marrink, S. J.; Risselada, H. J.; Yefimov, S.; Tieleman, D. P.; de Vries, A. H. The Martini Force Field: Coarse Grained Model for Biomolecular Simulations. *J. Phys. Chem. B* **2007**, *111*, 7812–7824.
34. Marrink, S. J.; Mark, A. E. Molecular Dynamics Simulation of the Formation, Structure, and Dynamics of Small Phospholipid Vesicles. *J. Am. Chem. Soc.* **2003**, *125*, 15233–15242.
35. Srinivas, G.; Klein, M. L. Molecular Dynamics Simulations of Self-Assembly and Nanotube Formation by Amphiphilic Molecules in Aqueous Solution: A Coarse-Grain Approach. *Nanotechnology* **2007**, *18*.
36. Hyde, S. T.; Barnes, I. S.; Ninham, B. W. Curvature Energy of Surfactant Interfaces Confined to the Plaquettes of a Cubic Lattice. *Langmuir* **1990**, *6*, 1055–1062.
37. Seifert, U.; Berndl, K.; Lipowsky, R. Shape Transformations of Vesicles—Phase-Diagram for Spontaneous-Curvature and Bilayer-Coupling Models. *Phys. Rev. A* **1991**, *44*, 1182–1202.
38. Childers, W. S.; Mehta, A. K.; Ni, R.; Taylor, J. V.; Lynn, D. G. Peptides Organized as Bilayer Membranes. *Angew. Chem., Int. Ed.* **2010**, *49*, 4104–4107.
39. Cenker, C. C.; Bucak, S.; Olsson, U. Nanotubes and Bilayers in a Model Peptide System. *Soft Matter* **2011**, *7*, 4868–4875.

40. Rzepiela, A. J.; Schafer, L. V.; Goga, N.; Risselada, H. J.; De Vries, A. H.; Marrink, S. J. Software News and Update Reconstruction of Atomistic Details from Coarse-Grained Structures. *J. Comput. Chem.* **2010**, *31*, 1333–1343.
41. Gunsteren, W. F. V.; Billeter, S. R.; Eising, A. A.; Hunenberger, P. H.; Kruger, P.; Mark, A. E.; Scott, W. R. P.; Tironi, I. G. *Biomolecular Simulations: The Gromos96 Manual and User Guide*; Verlag der Fachvereine Hochschulverlag AG: Zurich, Switzerland, 1996.
42. Zhou, R. H.; Huang, X. H.; Margulis, C. J.; Berne, B. J. Hydrophobic Collapse in Multidomain Protein Folding. *Science* **2004**, *305*, 1605–1609.
43. Liu, P.; Huang, X. H.; Zhou, R. H.; Berne, B. J. Observation of a Dewetting Transition in the Collapse of the Melittin Tetramer. *Nature* **2005**, *437*, 159–162.
44. Garcia, A. E.; Paschek, D. Simulation of the Pressure and Temperature Folding/Unfolding Equilibrium of a Small Rna Hairpin. *J. Am. Chem. Soc.* **2008**, *130*, 815–816.
45. Miyashita, N.; Straub, J. E.; Thirumalai, D. Structures of Beta-Amyloid Peptide 1-40, 1-42, and 1-55-the 672-726 Fragment of App-in a Membrane Environment with Implications for Interactions with Gamma-Secretase. *J. Am. Chem. Soc.* **2009**, *131*, 17843–17852.
46. Gao, Y. Q.; Yang, W.; Karplus, M. A Structure-Based Model for the Synthesis and Hydrolysis of Atp by F1-Atpase. *Cell* **2005**, *123*, 195–205.
47. Krone, M. G.; Hua, L.; Soto, P.; Zhou, R.; Berne, B. J.; Shea, J. E. Role of Water in Mediating the Assembly of Alzheimer Amyloid-Beta Abeta16-22 Protofilaments. *J. Am. Chem. Soc.* **2008**, *130*, 11066–11072.
48. Zuo, G.; Huang, Q.; Wei, G.; Zhou, R.; Fang, H. Plugging into Proteins: Poisoning Protein Function by a Hydrophobic Nanoparticle. *ACS Nano* **2010**, *4*, 7508–7514.
49. Wu, C.; Lei, H. X.; Duan, Y. Elongation of Ordered Peptide Aggregate of an Amyloidogenic Hexapeptide Nfgail Observed in Molecular Dynamics Simulations with Explicit Solvent. *J. Am. Chem. Soc.* **2005**, *127*, 13530–13537.
50. Wei, G. H.; Jewett, A. I.; Shea, J. E. Structural Diversity of Dimers of the Alzheimer Amyloid-Beta(25−35) Peptide and Polymorphism of the Resulting Fibrils. *Phys. Chem. Chem. Phys.* **2010**, *12*, 3622–3629.
51. Lindahl, E.; Hess, B.; van der Spoel, D. Gromacs 3.0: A Package for Molecular Simulation and Trajectory Analysis. *J. Mol. Model.* **2001**, *7*, 306–317.
52. Marrink, S. J.; Periole, X.; Tieleman, D. P.; de Vries, A. H. Comment on "on Using a Too Large Integration Time Step in Molecular Dynamics Simulations of Coarse-Grained Molecular Models" by M. Winger, D. Trzesniak, R. Baron and W. F. Van Gunsteren, Phys. Chem. Chem. Phys., 2009, 11, 1934. *Phys. Chem. Chem. Phys.* **2010**, *12*, 2254–2256.
53. Berendsen, H. J. C.; Postma, J. P. M; Vangunsteren, W. F.; Dinola, A.; Haak, J. R. Molecular-Dynamics with Coupling to an External Bath. *J. Chem. Phys.* **1984**, *81*, 3684–3690.
54. Levy, R. M.; Zhang, L. Y.; Gallicchio, E.; Felts, A. K. On the Nonpolar Hydration Free Energy of Proteins: Surface Area and Continuum Solvent Models for the Solute-Solvent Interaction Energy. *J. Am. Chem. Soc.* **2003**, *125*, 9523–9530.
55. Humphrey, W.; Dalke, A.; Schulten, K. VMD: Visual Molecular Dynamics. *J. Mol. Graph.* **1996**, *14*, 33–38.